Numerical simulation and experimental investigation of coaxiality change of laser cladding rotor shaft

Shirui Guo, Junhao Yu, Lujun Cui, Yinghao Cui, anlong Cao, WenhanZeng, and Yang Zhao

Abstract. To study the change of coaxiality of rotor shaft during laser cladding, a numerical simulation of the rotor shaft was carried out by ANSYS Workbench, and the temperature field and structure field of the rotor shaft were simulated and analyzed by indirect coupling of transient temperature field and transient structure field. The temperature distribution of the rotor shaft during laser cladding was obtained from the results of the temperature field. The maximum temperature is 2350°C, and the final temperature converges to about 2100°C. Then, the results obtained from the temperature field are entered into the structure field as loads, and the change of coaxiality of rotor shaft during laser cladding is obtained. Finally, the laser is used to clad Fe60 powder on the 45 steel rotor shaft, and the coaxiality of the rotor shaft after cladding is measured by Taylor cylindricity meter. The measurement results are basically consistent with the simulation results, and the error is <10%. It lays a good foundation for exploring the cladding mode or track that can maintain better coaxiality of rotor shaft in the process of laser cladding and is of great significance for the repair of damaged rotor shaft.

Keywords: laser cladding; rotor shaft; numerical simulation; coaxiality; deformation.

1 Introduction

Laser cladding is a kind of surface repair technology arising in the 1970s. After 20 or 30 years of development, laser cladding technology has gradually matured and become a hot surface technology. Laser cladding technology uses high-energy and high-density laser beams to melt the cladding material and the substrate surface to form a melting pool. After rapid cooling and solidification, a good metallurgical coating is formed to repair or modify the surface of the substrate so the use-value of the substrate can be maximized. Laser cladding has many advantages, such as fast processing speed, fast cooling and solidification speed, low dilution rate (generally <5%), high metallurgical bonding strength, flexible processing area, small thermal deformation of component, and so on. It is widely used in shipbuilding, military industry, mining machinery, and other industries.[1,2] In our common mechanical equipment, shaft parts are very common parts, which are mainly used to transfer torque and support gears, cams, and other transmission parts in mechanical equipment. Therefore, the performance of shaft components directly affects the stability and service life of mechanical equipment. As the supporting parts of transmission parts, shaft parts usually need to bear a very large load and are often subject to friction, corrosion, impact, and extrusion, resulting in wear, corrosion, fatigue pitting, and other forms of parts failure. If such parts were directly abandoned, it would waste resources and increase manufacturing costs, which violates the principle of sustainable development. Therefore, it is important to repair and reuse such parts by laser cladding technology.[3,4]

At present, Yao et al. established a thermal mechanical coupling finite element model of single-layer laser multichannel lap cladding and analyzed the temperature field and stress field in the process of laser cladding by finite element method. The results show that the process

parameters have a significant effect on the experimental results.[5] Liu et al. established a half finite element model to study the evolution of temperature field and stress field of wide beam laser single pass cladding. The results show that the laser power and scanning speed have important effects on the evolution of thermal field and stress field.[6] Zhang et al. simulated the temperature field and stress field of Fe-Mn-Si-Cr-Ni shape memory alloy monorail and multitrack cladding layers using the finite element analysis software ANSYS. Finally, the peak temperature of the cladding layer was 2600°C. The stress distribution of the coating is tension compression tension.[7] Geng et al. coated iron-based alloy powder on the surface of 45 steel. The heat transfer and temperature field distribution during laser cladding of iron-based alloy were numerically simulated by ANSYS Workbench. The parameters of laser cladding of 45 steel matrix iron-based alloy powder were determined.[8] The above authors basically obtained the temperature distribution law and stress distribution by simulating the temperature field and thermal stress coupling field in the laser cladding process, and they obtained the optimal processing parameters by combining the simulation with the experiment but did not study the deformation caused by the cladding process.

Shu et al. obtained the distribution law of temperature and thermal stress in the cladding process of worn shaft surface by the coupling analysis of temperature field and structural field in ANSYS, knowing that the thermal stress corresponds to the temperature gradient and further study explained that the stress is the main cause of microcracks and cracks.[9] However, the deformation of the shaft is not described. Huang et al. studied the temperature field distribution, stress field distribution, and deformation results of the stepped shaft by numerical simulation.[10] However, this paper only makes a simple numerical simulation of the stepped shaft and does not carry out experimental verification and quantitative expression of the deformation of the stepped shaft.

Based on the above research, the deformation law of the coaxiality (coaxiality: the deviation of the measured axis from the theoretical axis) of the rotor shaft is simulated by thermal mechanical coupling and experimental verification is carried out, which lays a good foundation for exploring the cladding mode or track that can maintain better coaxiality of the rotor shaft in the cladding process. It has important guiding significance for the repair of damaged rotor shafts.

2 Numerical Simulation of Temperature Field and Structure Field of Rotor Shaft

2.1 *Heat Source Model*

The laser heat source in laser cladding has a high energy density, which releases high temperature and rapidly melts the powder and part of the matrix material to form a molten pool, and then rapidly cools to form a cladding layer. The shape of the laser spot and the distribution of heat flux have a great influence on the results of temperature field and structure field. At present, the Gauss heat source model is commonly used, as shown in Fig. 1.

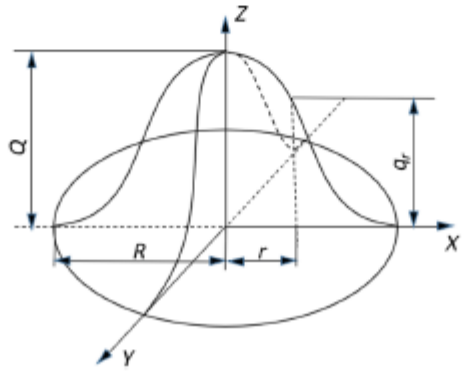

Fig. 1 Gaussian heat source model.

The expression is as follows:

$$q(r) = Q\exp\left(\frac{-3r^2}{R^2}\right), \tag{1}$$

where Q is the heat flux of the heat source center, r is the distance from a point to the center of the heat source, $q(r)$ is the heat flux at the distance r from the heat source center, and R is the radius of the heat source $R = \sqrt{x^2 + y^2}$.

2.2 *Thermodynamics Law and Temperature Field Control Equation in Laser Cladding*

The process of laser cladding is always accompanied by high temperature; there are three kinds of heat transfer modes in the process of laser cladding: heat radiation, heat conduction, and heat convection.[11–13] Since any object above absolute zero will produce thermal radiation, the radiation option in the boundary conditions will make the analysis highly nonlinear. To comprehensively consider the effects of radiation and convective heat transfer, a comprehensive surface convective heat transfer coefficient h_c is used:[14]

$$h_c = 2.41 \times 10^{-3}\varepsilon T^{1.61}. \tag{2}$$

2.2.1 *Law of heat convection*

Thermal convection occurs in the molten pool of laser cladding. Through the flowing medium in the molten pool, hot particles transfer heat from one place to another. Newton's cooling equation can describe the form of heat transfer. As shown below:

$$q_{\text{conv}} = h(T - T_0), \tag{3}$$

where h is the heat transfer and convection coefficient, T is the boundary surface temperature of the object, and T_0 is the medium ambient temperature.

2.2.2 *Law of heat conduction*

Heat conduction refers to the transfer of heat from the high-temperature part of an object to the low-temperature part of the same object or from one high-temperature object to another low-temperature object in contact with it. Heat conduction follows Fourier's law, and the basic form of heat conduction can be described as

$$q_{\text{cond}} = -k\frac{dT}{dx}, \tag{4}$$

where k is the thermal conductivity and dT/dx is the temperature gradient.

2.2.3 *Governing equation of temperature field*

$$\rho c\frac{\partial T}{\partial t} = \frac{\partial}{\partial x}\left(K_x\frac{\partial T}{\partial x}\right) + \frac{\partial}{\partial y}\left(K_y\frac{\partial T}{\partial y}\right) + \frac{\partial}{\partial z}\left(K_z\frac{\partial T}{\partial z}\right) + Q, \tag{5}$$

where ρ is the density of the material, unit kg/m^3, as a function of temperature; c is the specific heat capacity of the material, unit $\text{J/(kg} \times \text{K)}$, as a function of temperature; T is the distribution function of temperature field, unit K; t is the heat transfer time, units; K_x, K_y, K_z are the thermal conductivity units in x, y, zdirections, respectively; Q is the internal heat source, including phase change latent heat and heat source load.

2.3 *Establishment of Geometric Model and Mesh Generation*

2.3.1 *Establishment and hypothesis of a geometric model*

The geometric model was drawn by SOLIDWORKS. The radius of substrate axis of cladding position was 13 mm, the cladding width of the single-pass was 4 mm, the lap ratio was 40%, and the total cladding width was 9.6 mm. The materials of matrix and cladding layer are 45 steel and Fe-based alloy powder, respectively. The thermophysical parameters used for simulation are shown in Tables 1 and 2.

After the drawing is completed, it is imported into the "transient thermal" module and "transient structural" of ANSYS Workbench for numerical simulation and result analysis, and the following assumptions are made:

(1) The material is isotropic during cladding.
(2) The fluid flow in the molten pool and the vaporization of the material at high temperature are neglected.
(3) The thermal effect of temperature field accords with the classical heat transfer theory.
(4) The initial room temperature is defined as 22°C.
(5) To simplify the calculation, the slender axis is simplified as the optical axis.

The geometric plane model is shown in Fig. 2.

In Fig. 2, *L* is the total length of the rotor shaft, and its value is 580 mm; L1 is the clamping end during experiment and measurement, and it is also the reference cylinder for rotor shaft data acquisition; L2 is the cladding area of laser cladding experiment; L3 is the cylinder one for data acquisition; and L4 is the cylinder two for data acquisition.

2.3.2 *Meshing*

The above mathematical model is divided using the size control (sizing) in the mesh module of ANSYS Workbench. The matrix and cladding layer of rotor shaft is divided by hexahedron grid, among which the grid in the cladding area is refined, and the unit types are solid70 and solid185, both of which are hexahedron elements. The hexahedron element has eight nodes, so it has eight degrees of freedom. Solid70 is often used in the analysis of temperature fields. It can be used in

Table 1 Thermophysical property parameters of 45 steel.

Temperature (°C)	200	400	600	800	1000	1200
Specific heat (J/(g · k))	0.49	0.53	0.58	0.64	0.72	0.86
Thermal conductivity (W/(m · k))	42.90	41.72	39.52	37.04	34.48	32.10

Table 2 Thermophysical parameters of Fe based alloy powder.

Temperature (°C)	200	400	600	800	1000	1200
Specific heat (J/(g · k))	0.55	0.58	0.61	0.63	0.66	0.75
Thermal conductivity (W/(m · k))	11.23	12.01	12.75	13.55	14.26	15.0

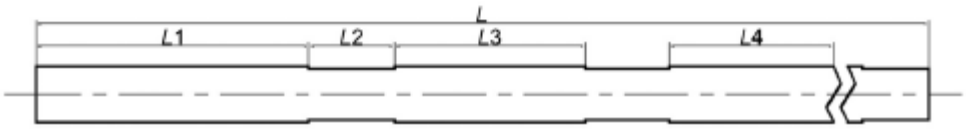

Fig. 2 Schematic diagram of rotor shaft.

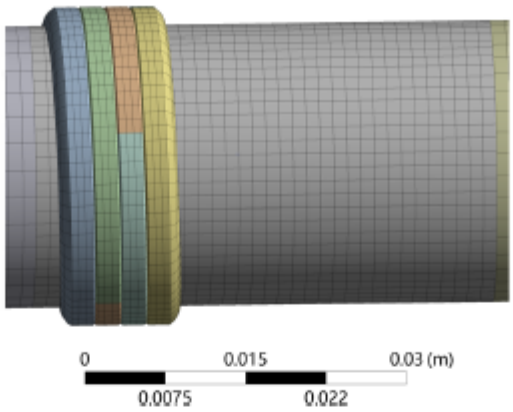

Fig. 3 Grid division display of geometric model.

both steady-state and transient thermal analysis modules. Solid70 unit can be converted to solid185 structure unit after getting node temperature value. Through the coupling of temperature field and structure field, the next step of structure field simulation results is analyzed. The mesh generation is shown in Fig. 3.

2.4 *Technology of Unit of Life and Death*

The birth and death element technology in ANSYS is the most commonly used technology for numerical simulation of laser cladding. Every unit of life and death is relative. The "dead" element does not mean that the element will be eliminated from the model, but the various physical parameters of the element will be multiplied by a very small factor so the values of various physical parameters are close to zero, which will not appear in the solution results of the model. On the contrary, the "birth" of the element is to restore all the physical parameters to their original values, which can be solved well. The birth and death element technology in ANSYS is to "kill" all the elements at the beginning. Then with the loading of laser heat source, these killed elements are activated one by one and appear in the solution results of the model.[13] In this way, ANSYS can be used to simulate the process of laser cladding.

2.5 *Simulation Results and Analysis of Temperature Field*

Due to the uneven heating and cooling process of laser cladding, the unequal phase transformation, and the temperature gradient caused by the different heating and cooling rates of the inner and outer layers of the parts, internal stress and thermal stress will be produced. The production of these stresses will make the parts produce plastic deformation and affect the function of the parts. To know the coaxiality deformation of rotor shaft parts under laser cladding, the method of indirect coupling between transient thermal and transient structural was used to carry out the numerical simulation. The temperature field simulation results and temperature distribution curves are shown in Figs. 4 and 5.

It can be seen from the temperature distribution nephogram and temperature distribution curve of temperature field simulation results that in the process of rotor shaft cladding, the temperature gradually increases at the beginning stage of cladding, and the temperature fluctuation is large. The maximum cladding temperature reaches about 2350°C. With the increase of time, the temperature curve gradually tends to be stable, and the temperature begins to converge, and finally stabilized at about 2100°C.

According to the law of heat transfer, there are three kinds of heat transfer modes: heat convection, heat conduction, and heat radiation. Therefore, when the rotor shaft is cladding, the high temperature in the cladding area will be transferred to other areas of the rotor shaft. To know the temperature distribution of the rotor shaft, cylinder one and cylinder two are selected on the rotor shaft to analyze the temperature field results. As shown in Figs. 6 and 7, the further away from the cladding area, the less affected by the cladding temperature, and the smaller the temperature

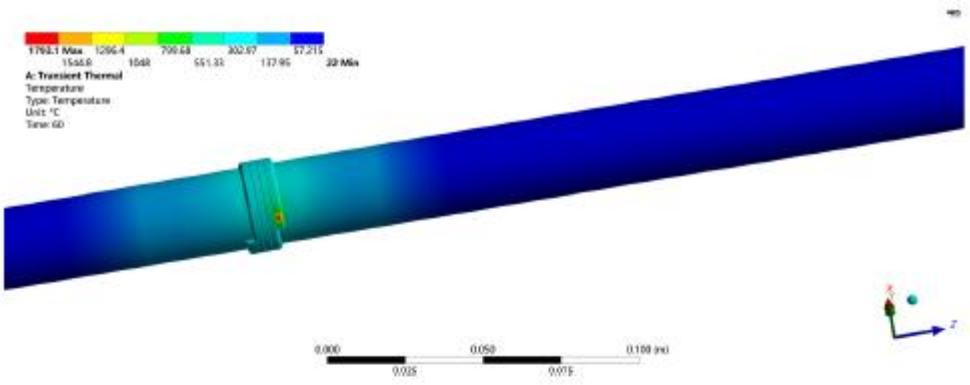

Fig. 4 Temperature distribution cloud.

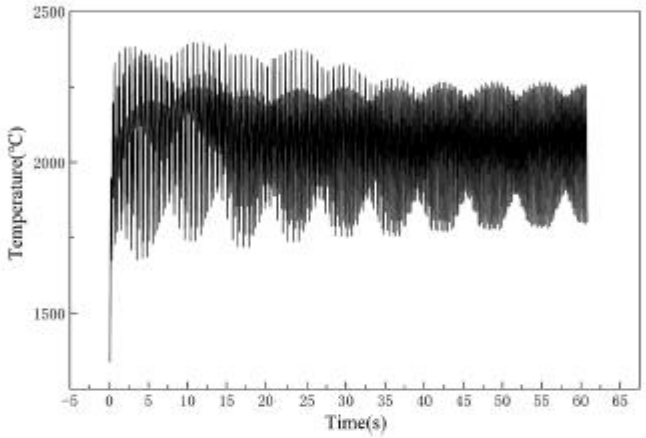

Fig. 5 Temperature distribution curve.

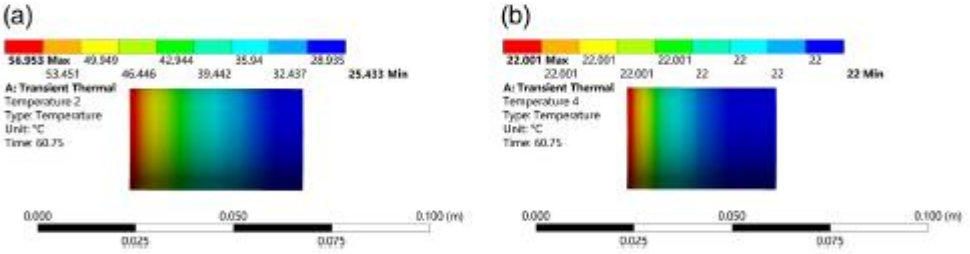

Fig. 6 Temperature distribution cloud of cylinder. (a) Temperature distribution of cylinder 1. (b) Temperature distribution of cylinder 2.

gradient was. Because the rotor shaft is too long, when the distance from the cladding area reaches a certain distance, the temperature of the rotor shaft cladding area cannot be conducted, and the temperature of the rotor shaft will be consistent with the room temperature.

2.6 *Simulation Results and Analysis of Structural Field*

At the end of the temperature field simulation process, the results obtained from the temperature field are entered into the structure field as the temperature load and the analysis and setting are carried out. The automatic time step and setting substep are turned on, and the fixed support is set at the bottom of the left end of the rotor shaft, and then the calculation of the structure field simulation process is carried out. The total deformation calculation results are shown in Figs. 8 and 9.

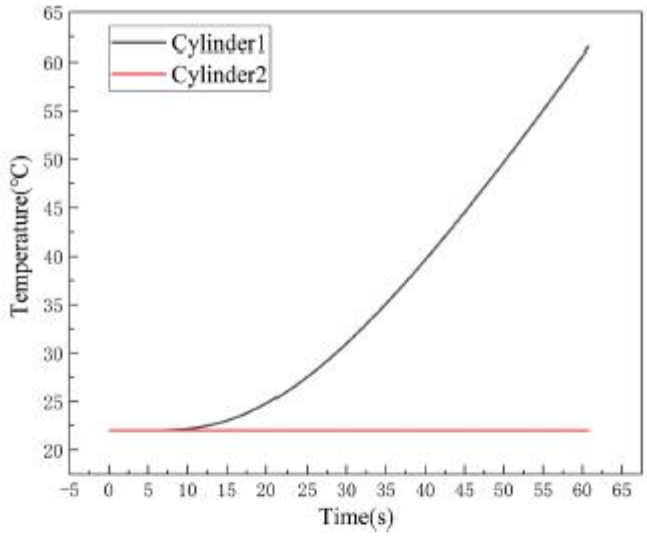

Fig. 7 Temperature change curve.

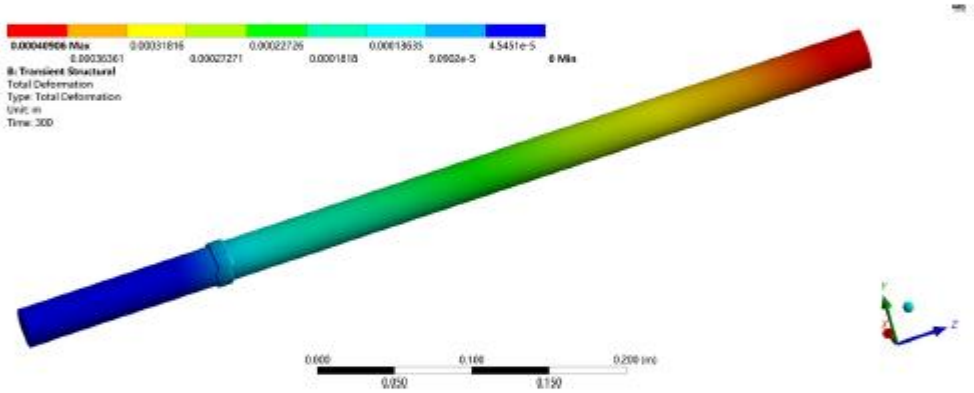

Fig. 8 Distribution of rotor shaft deformation.

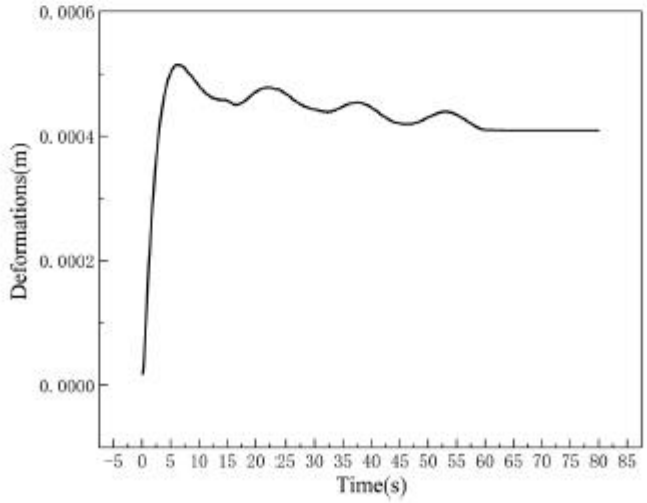

Fig. 9 Distribution curve of rotor shaft deformation.

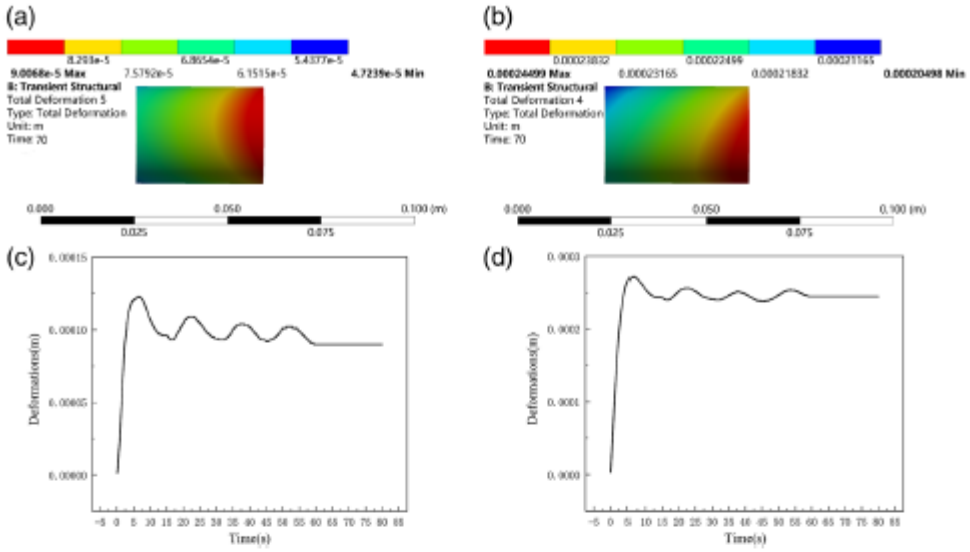

Fig. 10 Distribution of deformation. (a) Cloud image of deformation distribution of cylinder 1, (b) cloud image of deformation distribution of cylinder 2, (c) deformation curve of cylinder 1, and (d) deformation curve of cylinder 1.

According to the distribution nephogram and curve of the deformation of the rotor shaft, the bottom of the left end of the rotor shaft is the fixed support end, and the deformation is zero. Due to the influence of temperature load in the cladding process, the maximum deformation of the rotor shaft in the cladding process is 0.5 mm at the beginning of the first lap and decreases gradually with the cladding process. When the four laps are finished, the maximum deformation of the rotor shaft is stable at 0.4 mm. According to the nephogram of deformation distribution, the further away from the cladding area, the greater the initial deformation, and the maximum deformation is at the right end of the rotor shaft. To get the change of coaxiality of the rotor shaft at different positions during laser cladding, cylinder one and cylinder two are selected at the right end of the rotor shaft, and their deformation distribution nephogram and curve change graph are obtained from the simulation results, as shown in Fig. 10. The cylinder fixed at the left end of the rotor shaft is the reference cylinder, and the deformation of cylinder one and cylinder two are obtained, respectively. From the figure below, we can see that the deformation trend of cylinder one and cylinder two is the same as that of the rotor shaft. With the progress of cladding, the change gradually decreases from the maximum value and finally reaches stability. The final deformation of cylinder one and cylinder two is 90.06 and 244.73 μm. Therefore, from the simulation results, it can be known that in the process of laser cladding of rotor shaft, due to the existence of heat accumulation effect, thermal stress is generated in the process of cladding, resulting in the change of coaxiality of rotor shaft in the process of cladding. Moreover, the coaxiality changes with the distance from the cladding area.

3 Cladding Experiment of Rotor Shaft

3.1 *Experimental Materials*

The test base material is a rotor shaft made of 45 steel, and its chemical composition is shown in Table 3.

Table 3 Chemical composition of 45 steel (wt. %).

C	Mn	Si	Cr	Ni	Cu	P	S
0.42 to 0.50	0.50 to 0.80	0.17 to q0.37	≤ 0.25	≤ 0.25	≤ 0.25	≤ 0.040	≤ 0.045

Table 4 Composition of Fe60 alloy powder (wt. %).

C	B	Si	Cr	Ni	W	Fe
4.0 to 4.5	1.5 to 2.5	2.0 to 3.0	24.0 to 30.0	4.0 to 6.0	2.0 to 3.0	51.0 to 62.5

The alloy of the cladding layer is 100–200 mesh Fe-Cr-B-Si alloy powder, and its composition is shown in Table 4.

3.2 *Experimental Equipment and Methods*

High-precision cylindricity instrument (TALYROND 585lt-500) is used to measure and collect the original data of the rotor shaft after laser cladding. LDM8060 high-power semiconductor fiber-coupled laser was used in the laser cladding experiment. The spot diameter was 3 mm. The powder feeding method adopts rc-pgf-d-2 and double bin negative pressure powder feeder of China raycham (Nanjing Zhongke Yuchen) Company for four-way coaxial powder feeding. During the experiment, mcwl-150dt2 water cooler of China Tongfei Company was used to provide circulating cooling water for the laser and external optical path system, and nitrogen was used to protect the laser head and cladding environment. Single-layer cladding of Fe60 alloy powder was carried out on the circumferential surface of the rotor shaft, the lap ratio was 40%, the thickness of cladding layer was 2 mm, the cladding path was along the circumferential direction of the shaft, and the cladding process parameters were shown in Table 5. Before the experiment, the substrate was polished with sandpaper to remove the oxide layer on the surface, and then the surface of the substrate was cleaned with ethanol.

The total length of rotor shaft is 580 mm, the radius of matrix shaft at the cladding position is 13 mm, the cladding width of single pass is 4 mm, the lap rate is 40%, and the total cladding width is 9.6 mm. As shown in Fig. 11, the rotor shaft has good surface flatness after cladding, without obvious pores, cracks, and other defects.

3.3 *Experimental Data Measurement and Result Analysis*

The purpose of this experiment is to explore the radial deformation of the rotor shaft during laser cladding. To make the radial deformation of the rotor shaft more visible, the coaxiality of the rotor shaft is measured with a high-precision cylindricity instrument after the laser cladding experiment of the rotor shaft.

During the data measurement, the clamping end of the rotor shaft is cleaned up first. Then, the rotor shaft is put on the rotary table and clamped with a three-jaw chuck to fix one end of the

Table 5 Process parameters of laser cladding.

Cladding shaft material	Spot diameter (mm)	Lap rate (%)	Powder feeding quantity (mg/s)	Scanning speed (mm/s)	Laser power (W)	Protective gas
45 steel	3	40	15	6	1800	N_2

Fig. 11 Physical drawing of cladding.

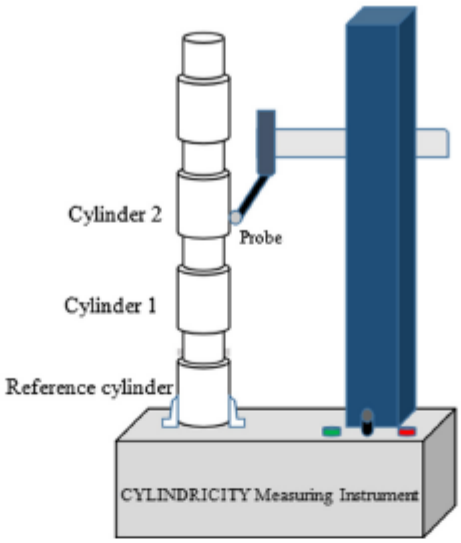

Fig. 12 Schematic diagram of experimental data measurement.

Table 6 Data sheet of coaxiality of rotor shaft after laser cladding.

Coaxiality after cladding (μm)	Cylinder (datum)	Cylinder 1	Cylinder 2
First measurement	0.00	83.72	227.43
Second measurement	0.00	83.88	230.58
Average value	0.00	83.80	229.005

rotor shaft to avoid the shaking of the rotor shaft in the measurement process and the measurement error. Finally, a suitable probe is selected to calibrate the rotor shaft and measure it.

When the rotor shaft is measured by the high-precision cylindricity meter, as shown in Fig. 12, it is necessary to select the corresponding cylindrical surface on the rotor shaft for cylindricity measurement. Among them, the cylinder at the fixed end is the reference cylinder, and this cylinder is taken as the reference to measure the coaxiality of cylinder one and cylinder two relative to datum cylinder. Four circular sections are selected on each cylinder surface for measurement. Through the coaxiality data of the rotor shaft after laser cladding, the deformation of the rotor shaft after laser cladding is quantitatively expressed. The coaxiality data of rotor shaft after cladding are shown in Table 6.

Based on the coaxiality data of the rotor shaft after cladding in the above table, it can be seen that the coaxiality of the two cylinders measured by the rotor shaft after laser cladding is 83.80 and 229.005 μm. It shows that due to the rapid heating and cooling process of laser cladding, the temperature gradient is too large, resulting in the concentration of thermal stress and internal stress, resulting in the plastic deformation of the rotor shaft and the change of its coaxiality. Moreover, the coaxiality change gradually increases away from the fixed end along the axial direction of the rotor shaft. It shows that laser cladding can change the coaxiality of the rotor shaft. The farther away from the fixed end, the greater the coaxiality change of the rotor shaft is.

3.4 *Comparative Analysis of Experimental Results and Simulation Results*

The deformation results of the rotor shaft obtained in the experiment are composed of machining error, measurement error, and laser cladding. The simulation results are based on certain assumptions; under the premise of the temperature field simulation results, the temperature is loaded into the structure field. The temperature gradient in the temperature field forms internal stress and

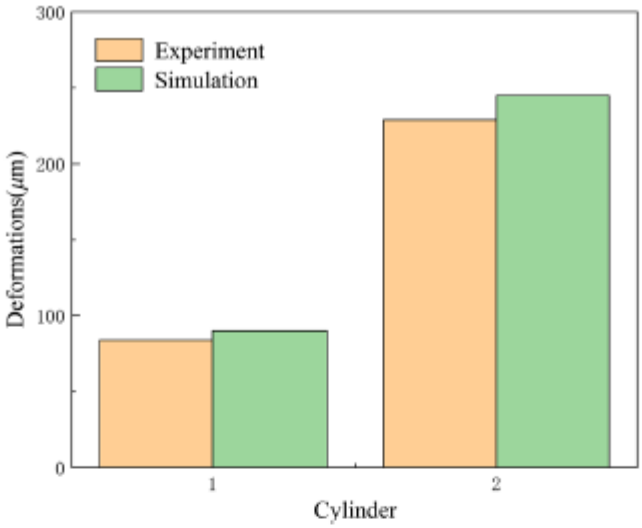

Fig. 13 Result data comparison chart.

thermal stress in the structure field and then makes the rotor shaft produce plastic deformation. The comparison results are shown in Fig. 13.

It can be seen from the above figure that the experimental results are very close to the simulation results, and the measured coaxiality deformation of cylinder one and cylinder two are 83.72 and 227.43 μm, respectively. And the deformation of cylinder one and cylinder two are 90.06 and 244.73 μm respectively. The error is within 10%.

4 Conclusion

In this paper, the temperature field and structural field of rotor shaft are numerically simulated using ANSYS finite element analysis software, and the temperature change and deformation during cladding are observed, analyzed, and verified by experiments. The uneven heating and cooling process of laser cladding, the unequal phase transformation and the temperature changes caused by the different heating and cooling speeds of the inner and outer layers of the parts will form a temperature gradient. The existence of the temperature gradient will produce complex internal stress and thermal stress on the rotor shaft, which will lead to plastic deformation and indirectly affect the coaxiality of the rotor shaft. The change of coaxiality will affect the mechanical properties of the rotor shaft and lead to the scrapping of the machine in serious cases. Therefore, understanding the change law of coaxiality of the rotor shaft in the process of laser cladding is of great significance to the repair of the damaged rotor shaft. The research method of this paper lays a good foundation for exploring the cladding mode or trajectory that can maintain better coaxiality of rotor shaft in the cladding process.

(1) In the simulation results of temperature field, the highest cladding temperature of the rotor shaft is about 2350°C. With the cladding process, the temperature curve gradually tends to be stable, and finally, the cladding temperature is stable at about 2100°C.
(2) In the simulation results of the structural field, the maximum deformation of the rotor shaft is 0.5 mm, and it is stable at 0.4 mm with the progress of cladding. The coaxiality of the two measured cylinders relative to the reference cylinder is stable at 90.06 and 244.73 μm.
(3) After the laser cladding experiment on the rotor shaft, the coaxiality of the two cylinders to the reference cylinder is 83.72 and 227.43 μm through the high precision cylindricity instrument (TALYROND 585lt-500).
(4) By comparing the simulation results with the experimental data, the relative error is <10%, verifying the accuracy of the simulation results.

Acknowledgments

This study was supported by the Key Scientific Research Project of Colleges and Universities in Henan Province (20A460033) and (20A460031), Henan Provincial Science and Technology Research Project (202102210068), special fund project for basic scientific research in Zhongyuan University of Technology (K2019QN006), Natural Science Foundation of Henan Province (202300410514), and general project of Henan Natural Science Foundation (212300410422), and open fund project of Anhui Key Laboratory of mine intelligent equipment and technology, Anhui University of Technology (kszn202003).

References

1. Z. P. Liu et al., "Application of laser cladding technology in high-speed rotor shaft repair," *Appl. Laser* **39**(5), 750–755 (2019).
2. N. Tamannar et al., "Progress in numerical simulation of the laser cladding process," *Opt. Lasers Eng.* **122**, 151–163 (2019).
3. Z. Q. Wang et al., "Application status of laser cladding technology in remanufacturing of shaft parts," *Mech. Eng. Mater.* **44**(11), 35–40 (2020).
4. L. D. Zhu et al., "Recent research and development status of laser cladding: a review," *Opt. Laser Technol.* **138**, 106915 (2021).
5. S. H. Yao et al., "Coupling analysis of temperature field and stress field of laser cladding die steel," *J. Phys. Conf. Ser.* **1676**(1), 012082 (2020).
6. H. M. Liu et al., "Numerical simulation of thermal and stress field of single track cladding in wide-beam laser cladding," *Int. J. Adv. Manuf. Technol.* **104**(9-12), 3959–3976 (2019).
7. Q. Zhang et al., "Numerical simulations of temperature and stress field of Fe-Mn-Si-Cr-Ni shape memory alloy coating synthesized by laser cladding," *Optic* **242**, 167079 (2021).
8. X. M. Geng, "Study on laser cladding process parameters of Fe-based alloy based on numerical simulation," *J. Phys. Conf. Ser.* **1948**(1), 012231 (2021).
9. L. S. Shu et al., "Numerical simulation and experiment of laser cladding process on worn shaft surface," *J. Mech. Eng.* **55**(09), 217–223 (2019).
10. Y. Huang et al., "Numerical simulation of temperature field and deformation during laser cladding repair of slender shaft parts," *Electromech. Equipment* **34**(4), 28–34 + 37 (2017).
11. L. Wang, "Laser cladding YSZ@Ni Finite element study on temperature field and stress field of coating," Nanchang Aviation University (2017).
12. G. Y. Peng, "Numerical simulation of temperature field and stress field of titanium alloy formed by laser selective melting," Huazhong University of Science and Technology (2018).
13. B. T. Chen, "Simulation and experimental research on temperature field and stress field of laser surface modification," Huazhong University of Science and Technology (2011).
14. D. Hu and R. Kovacevic, "Modelling and measuring the thermal behaviour of the molten pool in closed-loop controlled laser-based additive manufacturing," *Proc. Inst. Mech. Eng. Part B* **217**(4), 441–452 (2003).